THEORY, SIMULATION, AND COMPENSATION OF PHYSIOLOGICAL MOTION ARTIFACTS IN FUNCTIONAL MRI

Douglas C. Noll and Walter Schneider†*

Departments of *Radiology, *Electrical Engineering, and †Psychology
University of Pittsburgh, Pittsburgh, PA 15213
dnoll@cs.cmu.edu, SCHNEIDER@vms.cis.pitt.edu

ABSTRACT

Mapping the location of brain activity is a new and exciting application of magnetic resonance imaging (MRI). This application area has already seen the use of a variety of magnetic resonance image acquisition methods, including spin-warp, spiral k-space, and echo-planar imaging, each of which has its own advantages and disadvantages. In this paper, we examine physiological sources of image artifacts for functional brain mapping with MRI. In particular, we examine the nature of respiration-related signal changes in the brain and characterize the response of spin-warp and spiral k-space imaging to this source of artifacts. This characterization uses a model in which the respiration causes an undesired periodic structure in the Fourier domain of the image. We present simulation and experimental results to support this model and also present several methods to compensate for these effects so that these imaging methods can be used to generate artifact-free images.

1. INTRODUCTION

Functional brain imaging using MRI has received a great deal of attention from the MR research community in that past two years. The most common functional MRI technique uses T2*-weighting to sensitize the images to changes in blood oxygenation [1-4]. In this application, image intensity is generally compared between two different behavioral states to identify areas that have changed. These changes are often rather small, typically about 2%, which makes detection particularly sensitive to the presence of any image artifacts. Physiological processes, such as those related to the respiratory and cardiac cycles, are a major contributor to artifacts in abdominal imaging. While their effects are commonly ignored in anatomical brain imaging, in this paper, we show that they are large enough to affect functional brain imaging, where the signal changes of interest are very small.

This work was supported in part by the Whitaker Foundation.

Two data acquisition methods are examined below. Conventional or spin-warp imaging is a technique in which data is acquired in a raster format one line at a time in the object's Fourier space, which is also known as k-space. This imaging method is by far the most commonly available method, has well understood properties, and is very robust to magnetic field non-uniformities. In spiral k-space imaging, k-space is sampled along spiral trajectories [5-7], which allows larger areas of k-space to be acquired with each acquisition. This acquisition method has excellent properties with respect to motion and flow and can acquire data substantially faster than the spin-warp method; however, it is not as robust to magnetic field non-uniformity.

1.1. Physiological Variation in the Brain

The physiological variations can be seen in the brain by examining the MR signal averaged over a slice at a late gradient echo time (the free induction decay (FID) at 40 ms). Fig. 1 contains the slice averaged signal for a volunteer performing a breath-holding exercise, clearly showing the component due to respiration. During the breath-hold, the cardiac component is more apparent.

In a number of studies that included different subjects and slice orientations, only the respiratory effect in the received phase was consistently present. Given that respiration is relatively slow compared to our imaging capabilities, we were able to examine this effect in detail. By examining the response at different echo times, we determined that the size of respiratory phase variations increases approximately linearly with the echo time. The respiratory phase variations, therefore, are probably caused by variations in resonant frequency. In gradient echo imaging, the accumulated image phase is:

$$\angle I = \gamma \Delta B(t) T_E \tag{1}$$

where γ is the gyromagnetic ratio, ΔB is the change in magnetic field, and T_E is the echo time. For example, a 1 Hz shift in the resonant frequency (0.016 ppm at 1.5 T) causes

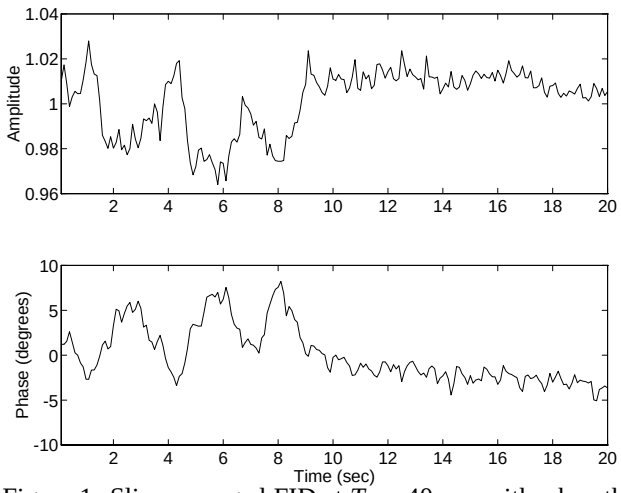

Figure 1: Slice averaged FID at T_E = 40 ms, with a breath-hold at t = 9 sec.

14 degree shift in the phase of the received signal at T_E = 40 ms.

We also examined the spatial distribution of respiratory-related phase variations in the brain by creating images rapidly and finding the average difference between images taken at peak inspiration and expiration. As seen in Fig. 2, the phase function varies smoothly with the largest effects at the inferior surface of the brain. The size of these changes in the brain are modest - a typical range is 0.15 Hz at the superior edge of the brain to 1 Hz in the temporal lobes (2 to 14 degrees at a 40 ms T_E).

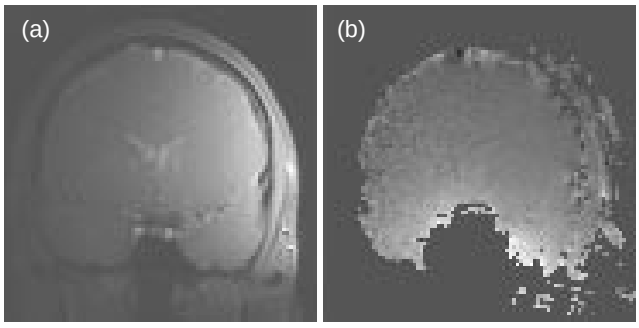

Figure 2: Distribution of the respiratory-related changes in resonant frequency for a coronal slice through the brain.

The phase variations are also present outside the brain and in phantoms, with particularly large changes, 5 Hz (70 degrees) or more, occurring in phantoms positioned just above the shoulders. This indicates that respiration probably does not cause changes in the MR properties of brain tissue, but causes changes in the magnetic distribution through the body and head. The likely source of this is susceptibility effects of movement of the chest wall and organs in the chest.

2. THEORETICAL MODEL OF RESPIRATION EFFECTS

The magnetic field variations related to respiration cause a temporally and spatially dependent phase function to be applied to the object. The time for each data acquisition (5-50 ms) is small relative to the time-scale of respiration. The respiratory-related phase function, therefore, can be assumed to be constant during each acquisition interval, and the acquired data corresponds to the desired object multiplied times some perturbation function. For functions that are very smooth, we can assume a *uniform bulk variability model*. In this model, we assume that all magnitude and phase perturbations apply uniformly to the entire object.

2.1. Spin-Warp Acquisition

One acquisition method that is well suited for examination using this model is the spin-warp method. Since the uniform bulk variability model affects all samples for any given line through k-space in exactly the same way, the spin-warp method can be evaluated using a one-dimensional model. The magnitude variation is modeled as a multiplicative weighting:

$$V_m(t) = 1 + A_m cos(2\pi f\, t + \phi_m) \qquad (2)$$

where $f = NT_R f_0$, N is the number of lines through k-space, T_R is the scanner repetition time, f_0 is the temporal frequency of the physiologic variation, and t is the time at which a particular line through k-space is acquired. This results in a the following final image:

$$\begin{aligned} I_m(x) &= |m(x) * v_m(x)| \\ &\approx m(x) + 0.5A_m cos(\phi_m)[m(x-f) + m(x+f)] \end{aligned} \qquad (3)$$

where $m(x)$ is the desired object, which has been assumed to be real, and $v_m(x)$ is the Fourier transform of Eqn. 2. The approximation of Eqn. 3 results from suppression of the component that is out-of-phase with the desired object due to the non-linear behavior of the magnitude operator when $A_m \ll 1$ [8, 9]. A similar analysis can be performed on a model of the phase variation:

$$\begin{aligned} V_p(t) &= exp(iA_p cos(2\pi f\, t + \phi_p)) \\ &\approx 1 + iA_p cos(2\pi f\, t + \phi_p) \end{aligned} \qquad (4)$$

by keeping only the low order terms ($A_p \ll 1$). This results in the following final image:

$$\begin{aligned} I_p(x) &= |m(x) * v_p(x)| \\ &\approx m(x) + 0.5A_p sin(\phi_p)[-m(x-f) + m(x+f)] \end{aligned} \qquad (5)$$

These variations, therefore, result in the desired object, $m(x)$, plus weighted and shifted versions of the object. The

weighting and sign at which these objects are added depends upon the temporal phase (ϕ_m or ϕ_p) of the variation with respect to the scanning period. If no steps are taken to synchronize the acquisition with the physiological cycle, then the temporal phases will vary randomly from trial to trial. The artifactual signal component will then vary in sign and magnitude from trial to trial leading to obvious artifacts when subtracting images from two different behavioral states.

The distance that the artifactual component is shifted by an amount proportional to f : for a typical respiration rate of 12/min. and cardiac rate of 60/min., T_R = 100 ms, and N = 128 lines through k-space, the size of the shifts are 2.5 and 13 pixels, respectively. At this T_R, the respiratory variations cause primarily edge effects while the cardiac variations can cause large object shifts that might appear as low spatial frequency variations. Image acquisition parameters also affect the artifacts. For instance, a five-fold increase in the scanner repetition time changes relative frequency (f), making shifts of the object five times larger (13 and 64 pixels, respectively).

Eqns. 3 and 5 above give the response to perturbations in the received magnitude and phase when superimposed on the object. Since the response includes shifted copies of the original object, the artifacts should also appear in the image background. The combined response for magnitude and phase in the object background, neglecting higher order terms, is:

$$I(x) \approx 0.5\left[\sqrt{A_m^2 + A_p^2 + 2A_mA_p sin(\Delta\phi)}m(x-f) + \sqrt{A_m^2 + A_p^2 - 2A_mA_p sin(\Delta\phi)}m(x+f)\right] \quad (6)$$

where $\Delta\phi = \phi_m - \phi_p$. Since the temporal relationship between magnitude and phase signals should remain constant, the artifact contribution in the image background will remain constant. Therefore, we would predict that there will be no visible artifacts in the background of the subtracted images. In the example of Fig. 1, the magnitude and phase signals appear to be exactly out-of-phase ($\Delta\phi \approx \pi$). In this case, the expression for artifacts in the image background reduces an expression with no dependence on the temporal phase of the physiological cycle:

$$I(x) \approx 0.5\sqrt{A_m^2 + A_p^2}[m(x-f) + m(x+f)]. \quad (7)$$

3. SIMULATION OF ARTIFACTS

While the measured size of the physiological variations in the brain are quite small, the desired signal changes are similarly quite small. The following simulation studies show these variations can cause changes in image intensity as large as or larger than the expected signal changes from a functional imaging experiment. As above, phase and magnitude variations are assumed to apply uniformly to the k-space data of the desired object. The simulations were performed using two different recordings of the FID with those phase and magnitude perturbations applied to artificial k-space data. Like the example of Fig. 1, the data used for the simulations is dominated by respirations effects, though in some cases we have observed a much larger cardiac component. The results are presented as differences between the two simulated objects.

3.1. Spin-warp Imaging

As in the theoretical study above, a one-dimensional study can be used to estimate the effects on the spin-warp imaging method. The spin-warp simulations assumed acquisition of 64 lines through k-space. Depending on the T_R, the respiratory variations can cause image artifacts that vary in size and nature. In short T_R studies, the respiratory phase variations cause mainly edge artifacts as demonstrated in the 100 ms T_R simulation of Fig.3 (solid line). Cardiac variations and noise contribute to the other effects that are visible. Also, as predicted by the theoretical model, in the object background (< 20 and > 45 on the horizontal scale) there are no visible artifacts. This is because the artifactual component in the background is exactly the same for both trials. In longer T_R studies, the respiratory phase variations cause larger shifts of the object as demonstrated in the 1000 ms T_R simulation (dashed line). These can appear as low-spatial frequency bands of low and high signal intensity, an artifact that we have commonly seen in our functional imaging studies.

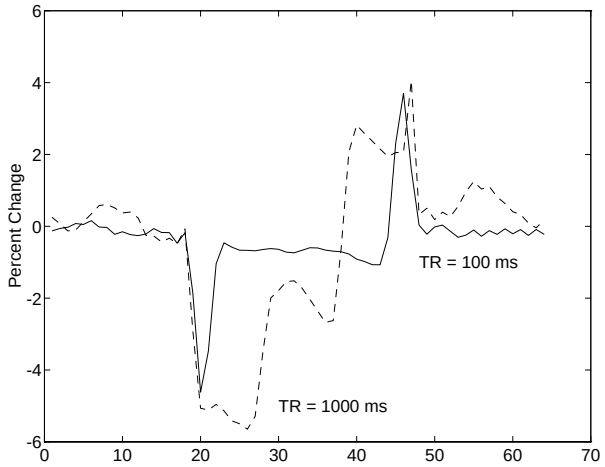

Figure 3: Plot of a representative difference between the two simulated objects using spin-warp acquisitions with T_R = 100 ms and 1000 ms. The simulation object was a rectangle function located approximately between 20 and 45 on the horizontal scale.

3.2. Spiral k-space Imaging

Due to the inherent two-dimensional (2D) nature of spiral acquisitions, it is necessary to conduct 2D simulations, in this case, of a square object. The spiral data acquisition assumed acquisition of 8 interleaved spiral trajectories. In this case, artifacts are minimized by using a short T_R, making the acquired data more consistent. In the short T_R (100 ms) simulation of Fig.4(a), the respiratory phase variations cause very little inconsistency of the data and thus, very little artifact. The only artifactual signal here is an overall scaling of the object resulting primarily from global magnitude variation of the received signal. In longer T_R studies, the respiratory phase variations cause large image artifacts in the 1000 ms T_R simulation of Fig.4(b). Unlike the spin-warp data acquisition, this model does not predict that that there will be no artifacts in the image background.

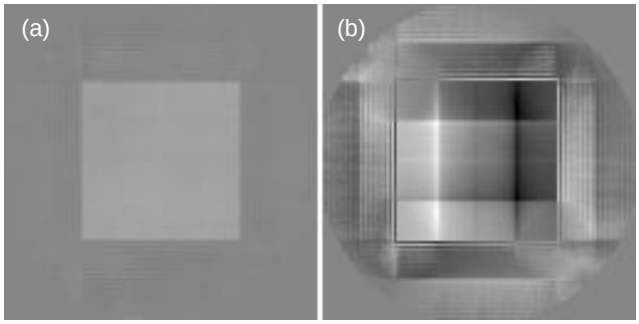

Figure 4: Representative difference images between the two simulated objects using spiral k-space acquisitions with T_R = (a) 100 ms and (b) 1000 ms. The simulation object is a square, similar to that seen in (a).

4. COMPENSATION STRATEGIES

Respiration and cardiac artifacts are have been studied in the context of abdominal imaging. Perhaps the most common method for respiratory compensation in the abdomen is reordering of phase encoding lines to particular locations in the respiratory cycle [5,6]. This can easily be applied to the gradient echo pulse sequence commonly used in conventional functional imaging studies; however, it is most effective when the acquisition interval spans several cycles of respiration. Also, it is difficult to apply effectively to rapid scanning techniques like spiral k-space imaging. The most common cardiac artifact suppression technique is gating acquisition to the cardiac cycle. We have found that this is ineffective for functional MRI since normal variations in cardiac timing contribute new image artifacts.

As described by the theoretical model, the image artifacts are present because the temporal phase of the physiological cycle varies from trial to trial. Another approach, then, is the synchronize the start of acquisitions with a physiological cycle. This approach would be most effective if the physiological cycles are very consistent so that the effects will be exactly the same for any two acquisitions. For a longer acquisition period, synchronization is likely to degrade. Also, as a practical matter, this approach can only be used to address either respiratory or cardiac cycles, but not both. Below, we describe another artifact compensation technique that can be used alone or in combination with the other techniques.

4.1. Navigator Corrections

Based on the uniform bulk variability model, we propose a new strategy to compensate for respiratory effects in the brain using navigator echoes to measure the received signal phase [10, 11]. This method requires no external monitoring of respiration and can easily be applied to a variety of different imaging methods. Since the respiratory phase variations in the brain are smoothly varying, corrections can be made using a single sample of the FID and using that phase term to correct the phase of corresponding samples. Also, since the respiratory phase variations are due to off-resonance effects navigator samples can be acquired at one echo time and be projected to the echo time of the image acquisition.

Navigator corrections have been applied to spin-warp data in which the phase of the FID was sampled with T_E = 20 ms and the image samples, acquired with T_E = 40 ms, were corrected using $2\times$ the measured phase. Fig. 5 demonstrates effectiveness for the difference of a single pair of images in motor cortex. Observe that the artifacts in the uncorrected data have the same properties described by the theoretical and simulation models. In particular, the largest effects are near the edges, as would be expected for a T_R = 200 ms study, and there are no visible artifacts in the image background.

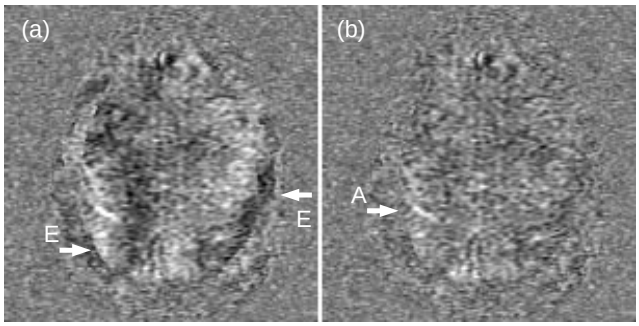

Figure 5: Difference of a single pair of images in motor cortex (a) without and (b) with navigator corrections for spin-warp imaging with T_R = 200 ms. Edge artifacts are labeled (E) and the activation area is labeled (A).

Navigator corrections have also been applied to spiral k-space data. Since every spiral acquisition begins at the center of k-space, the FID is already sampled with each acquisition.

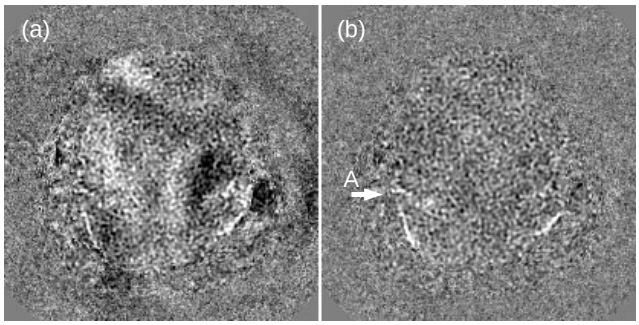

Figure 6: Difference of a single pair of images in motor cortex (a) without and (b) with navigator corrections for spiral k-space imaging with T_R = 500 ms. Area of activation is labeled (A).

Application of the navigator technique to spiral imaging, therefore, requires no additional data or any modification to the acquisition sequence. The timing of the sample of the FID also coincides with the data acquisition making the measurement more accurate than projecting the phase from a different echo time. Fig. 6 shows application of the navigator correction to data acquired using the spiral k-space technique.

5. CONCLUSIONS

Variations in resonant frequency due to movement of the chest and its organs during respiration are apparent in the brain and can cause artifacts in functional images. A simple uniform bulk variability model can be used to understand these artifacts, to predict the influence on different acquisition trajectories and to derive compensation strategies. One such strategy, described above, is the navigator correction technique which can be used to generate artifact-free images for functional MRI.

6. REFERENCES

[1] K. R. Thulborn, J. C. Waterton, P. M. Matthews, and G. K. Radda, "Oxygenation dependence of the transverse relaxation time of water protons in whole blood at high field," *Biochem. Biophys. Acta*, vol. 714, pp. 265–270, 1982.

[2] S. Ogawa, T. M. Lee, A. S. Nayak, and P. Glynn, "Oxygenation-sensitive contrast in magnetic resonance image of rodent brain at high magnetic fields," *Magn. Res. Med.*, vol. 14, pp. 68–74, 1990.

[3] K. K. Kwong, J. W. Belliveau, D. A. Chesler, *et al.*, "Dynamic magnetic resonance imaging of human brain activity during primary sensory stimulation," *Proc. Nat. Acad. Sci. USA*, vol. 89, pp. 5675–5679, 1992.

[4] S. Ogawa, D. W. Tank, R. Menon, *et al.*, "Intrinsic singal changes accompanying sensory stimulation: functional brain mapping using MRI," *Proc. Nat. Acad. Sci. USA*, vol. 89, p. 5951, 1992.

[5] C. B. Ahn, J. H. Kim, and Z. H. Cho, "High-speed spiral-scan echo planar NMR imaging-I," *IEEE Trans. Medical Imag.*, vol. MI-5, pp. 2–7, 1986.

[6] C. H. Meyer, B. S. Hu, D. G. Nishimura, and A. Macovski, "Fast spiral coronary artery imaging," *Magn. Res. Med.*, vol. 28, pp. 202–213, 1992.

[7] D. C. Noll, J. D. Cohen, C. H. Meyer, and W. Schneider, "Spiral k-space MRI of cortical activation," *J. Magn. Res. Imag.*, in press, 1994.

[8] A. B. Carlson, *Communication Systems*. New York: McGraw Hill, third ed., 1986.

[9] D. C. Noll, D. G. Nishimura, and A. Macovski, "Homodyne detection in magnetic resonance imaging," *IEEE Trans. Medical Imag.*, vol. MI-10, no. 2, pp. 154–163, 1991.

[10] D. C. Noll, W. Schneider, and J. D. Cohen, "Artifacts in functional MRI using conventional scanning," in *Proc., 12th Ann. Mtg. Soc. Magn. Res. Med.*, p. 1407, 1993.

[11] X. Hu and S. G. Kim, "Reduction of signal fluctuations in functional MRI using navigator echoes," *Magn. Res. Med.*, vol. 31, pp. 495–503, 1994.